Published OnlineFirst June 30, 2016; DOI: 10.1158/1535-7163.MCT-15-0554

Small Molecule Therapeutics

Molecular Cancer Therapeutics

Synthetic Lethal Targeting of *ARID1A*-Mutant Ovarian Clear Cell Tumors with Dasatinib

Rowan E. Miller[1,2], Rachel Brough[1,2], Ilirjana Bajrami[1,2], Chris T. Williamson[1,2], Simon McDade[3], James Campbell[1,2], Asha Kigozi[1,2], Rumana Rafiq[1,2], Helen Pemberton[1,2], Rachel Natrajan[2], Josephine Joel[4], Holly Astley[4], Claire Mahoney[4], Jonathan D. Moore[4], Chris Torrance[4], John D. Gordan[5], James T. Webber[5], Rebecca S. Levin[6], Kevan M. Shokat[6,7], Sourav Bandyopadhyay[5], Christopher J. Lord[1,2], and Alan Ashworth[1,2]

Abstract

New targeted approaches to ovarian clear cell carcinomas (OCCC) are needed, given the limited treatment options in this disease and the poor response to standard chemotherapy. Using a series of high-throughput cell-based drug screens in OCCC tumor cell models, we have identified a synthetic lethal (SL) interaction between the kinase inhibitor dasatinib and a key driver in OCCC, *ARID1A* mutation. Imposing ARID1A deficiency upon a variety of human or mouse cells induced dasatinib sensitivity, both *in vitro* and *in vivo*, suggesting that this is a robust synthetic lethal interaction. The sensitivity of *ARID1A*-deficient cells to dasatinib was associated with G_1–S cell-cycle arrest and was dependent upon both p21 and Rb. Using focused siRNA screens and kinase profiling, we showed that *ARID1A*-mutant OCCC tumor cells are addicted to the dasatinib target YES1. This suggests that dasatinib merits investigation for the treatment of patients with *ARID1A*-mutant OCCC. *Mol Cancer Ther; 15(7); 1472–84. ©2016 AACR.*

Introduction

Ovarian clear cell carcinomas (OCCC) comprise between 5 and 25% of all epithelial ovarian cancers and are often associated with endometriosis (1). Patients with advanced OCCC generally respond poorly to standard platinum-based chemotherapy and have a median 5-year survival rate of less than 32% (2, 3). Recently, comprehensive DNA sequencing of OCCCs has led to the identification of likely driver mutations in this disease (4, 5). The most commonly recurrent genetic event in OCCC is somatic mutation in the tumor suppressor gene *ARID1A* (AT-Rich Interactive Domain-containing protein 1A) which is present in up to 57% of patients (4, 5). A significant proportion of the tumor-associated somatic *ARID1A* mutations in OCCC are frame-shift insertion/deletion mutations or nonsense mutations that are predicted to result in premature truncation of the protein (4, 5). In addition to being recurrently mutated in OCCC, frame-shift insertion/deletion mutations and nonsense mutations in *ARID1A* have also been identified in multiple other cancer types such as gastric cancer, renal clear cell cancer, and pancreatic tumors (6). Loss of ARID1A expression has also been associated with a shorter progression-free survival and resistance to platinum-based chemotherapy in OCCC patients (7).

The best-characterized role of the ARID1A protein is as a component of the BAF SWI/SNF chromatin-remodeling complex. The BAF complex plays a key role in modifying the position of nucleosomes on DNA (8–10) and in doing so likely regulates the access of additional proteins to DNA (8). The composition of the BAF complex includes: (i) an ATP-dependent DNA helicase, encoded by the *SMARCA4/BRG1* or *SMARCA2/BRM* genes; (ii) ARID1A or ARID1B, which each encompass an ARID DNA–binding domain; and (iii) a series of additional accessory subunits such as SMARCB1, SMARC1 and 2, SMARCD1-3, SMARCE1, ACTL6A and DFP1–3 (8, 11). ARID1A dysfunction has been associated with a relatively diverse set of phenotypes including defects in cell differentiation, alterations in the control of cell proliferation, as well as defects in the repair of DNA (9, 10, 12, 13). However, a precise molecular understanding of how defects in ARID1A lead to each of these phenotypes is not yet clear.

Given the high prevalence of *ARID1A* mutations in OCCC, identifying drugs that selectively target *ARID1A*-mutant tumor cells could potentially inform the development of new therapeutic approaches to this disease. Recently the methyltransferase, EZH2 and PARP inhibitors have been proposed as therapeutic targets in ARID1A-mutant tumors (14, 15) and synthetic lethality

[1]The CRUK Gene Function Laboratory, The Institute of Cancer Research, London, United Kingdom. [2]Breakthrough Breast Cancer Research Centre, The Institute of Cancer Research, London, United Kingdom. [3]Centre for Cancer Research and Cell Biology, Queen's University Belfast, Belfast, United Kingdom. [4]Horizon Discovery, Waterbeach, Cambridge, United Kingdom. [5]UCSF Helen Diller Family Comprehensive Cancer Center, University of California, San Francisco, San Francisco, California. [6]Cellular and Molecular Pharmacology University of California, San Francisco, San Francisco, California. [7]Howard Hughes Medical Institute, University of California, San Francisco, San Francisco, California.

Note: Supplementary data for this article are available at Molecular Cancer Therapeutics Online (http://mct.aacrjournals.org/).

Current address for C. Torrance: PhoreMost, 23 Cambridge Science Park, Milton Road, Cambridge CB4 0EY, United Kingdom; and current address for A. Ashworth: UCSF Helen Diller Family Comprehensive Cancer Center, University of California, San Francisco, San Francisco, CA 94158.

Corresponding Author: Christopher J. Lord, The Institute of Cancer Research, 237 Fulham Road, London SW3 6JB, United Kingdom. Phone: 4420-7153-5190; Fax: 4420-7153-5332; E-mail Chris.Lord@icr.ac.uk; and Alan Ashworth, UCSF Helen Diller Family Comprehensive Cancer Center, University of California, San Francisco, San Francisco, CA 94158. E-mail: Alan.Ashworth@ucsf.edu

doi: 10.1158/1535-7163.MCT-15-0554

Published OnlineFirst June 30, 2016; DOI: 10.1158/1535-7163.MCT-15-0554

between ARID1A and ARID1B has also been described (16). Here, we describe a high-throughput functional genomics approach to screen a series of clinically used drugs with the intention of identifying novel *ARID1A* synthetic lethal effects (17) that operate in OCCC. By profiling drugs that are either already used in the clinical management of cancer or compounds with targets that are currently in late-stage development, we also aimed to identify ARID1A synthetic lethal approaches that could potentially be rapidly translated in the clinic.

Materials and Methods

Reagents and cell lines

Dasatinib was purchased from Selleck chemicals. Additional drugs and small-molecule inhibitors used in this study are listed in Supplementary Table S1. ES2 and TOV21G were obtained from the ATCC. RMG-1, SMOV2, KOC7C, HCH1, OVAS, OVISE, OVMANA, OVTOKO, and KK were provided by Dr. Hiroaki Itamochi (Tottori University School of Medicine, Yonago, Japan). Ovarian clear cell lines were grown in RPMI with 10% FCS. The identity of cell lines was confirmed by STR typing using the StemElite Kit (Promega) in March 2013 and where appropriate, profiles were confirmed using the Children's Oncology Group (COG) Cell Culture and Xenograft Repository bank (http://strdb.cogcell.org) or JCRB cell bank (http://cellbank.nibiohn.go.jp/english/). ARID1A HCT116 were grown in McCoy media with 10% (v/v) FCS. *Arid1a*-null and wild-type mouse embryonic stem cells were provided by Dr. Zhong Wang (Harvard Medical School, Boston, MA; ref. 9) and grown on gelatin-coated plates in DMEM with 10% (v/v) FCS supplemented with 0.1 mmol/L nonessential amino acids, 1 mmol/L sodium pyruvate, 0.1 mmol/L beta-metcaptothanol, and 2,000 U LIF/mL. All cell lines were routinely confirmed as being mycoplasma negative using the MycoAlert Kit (Lonza) throughout experimentation.

High-throughput drug screen

Cell lines were profiled using a customized drug library (Supplementary Materials and Methods) containing 68 compounds (Supplementary Tables S2 and S3). Cells were plated at a density of 250 or 500 cells per well. Twenty-four hours later, media containing drug library were added to adherent cells. On day seven, cell viability in each well was estimated using CellTiter-Glo (Promega). Luminescence data was log2 transformed and centered on a per plate basis according to the plate median value. Z prime >0.3 and r^2 >0.75 were used to define acceptable screen data. Where appropriate, surviving fractions were calculated relative to DMSO-treated wells and these data were used to generate AUC and SF_{50} data.

Cell-based assays

Short-term drug exposure assays were performed in 96-well plates. Cells were plated at a density of 250–500 cells/well and drug added at the indicated concentration 24 hours later. Cell viability was estimated after seven days using Cell-Titre Glo (Promega). Surviving fractions (SF) were calculated relative to DMSO-treated wells, and drug sensitivity curves plotted.

Clonogenic assays were performed in triplicate in 6-well plates. OCCC cell lines were plated at a density of 500 cells/well and mouse embryonic stem (ES) cells were plated at a density of 2,000 cells per well on gelatin-coated plates. Media containing dasatinib at the indicated concentrations were replaced every three days. After 14 days, cells were fixed in 10% trichloroacetic acid and stained with sulforhodamine-B prior to counting.

siRNA experiments

A 384-well plate arrayed siRNA library targeting 784 genes (Dharmacon) was used (gene list described in Supplementary Table S4) or a bespoke Dharmacon siRNA library of dasatinib targets. Each well either contained a SMART pool (four distinct siRNA species targeting different sequences of the target transcript combined) or a single siRNA species. Additional positive (siPLK1) and negative [siCON1, siCON2 and Allstar (Dharmacon and Qiagen, respectively)] controls were also added to each plate. Cells were reverse transfected using Dharmafect4 (Dharmacon). Forty-eight hours after transfection, media containing dasatinib or the drug vehicle, DMSO, were added to the plates. After seven days, cell viability in each well was estimated using a CellTiter-Glo assay. Data were processed as described in Supplementary Materials and Methods and as in ref. 18.

Dasatinib bead proteomics

Inhibitor bead proteomics was performed as described previously (19, 20). Dasatinib was covalently linked to ECH sepharose 4B using EDC and then 1 mg of precleared cell lysate was rotated with 50 μL of dasatinib bead slurry for three hours. Beads were washed twice with cold binding buffer and then an additional three times with binding buffer with reduced NaCl minus detergent. Proteins were eluted with 6 mol/L urea and trypsinized, desalted, and analyzed by LC-MS/MS on a Thermo LTQ Orbitrap Velos. Spectra were searched using Protein Prospector and label-free quantitation performed with Skyline. Significance of effects was determined using MS Stats (21).

Protein analysis

Cells were lysed, electrophoresed, and immunoblotted as described previously (22). We used the following antibodies: ARID1A [Bethyl A301-040A (human) and Santa Cruz Biotechnology sc-32761 (mouse)] α-Actinin (A5044, Sigma), Actin (sc-1616, Santa Cruz Biotechnology), β-Tubulin, (2146, Cell Signaling Technology), YES1 (3201S, Cell Signaling Technology), and CDKN1A (2947, Cell Signaling Technology). All secondary antibodies were horseradish peroxidase conjugated. Primary antibodies were used at a concentration of 1:1,000 and secondary antibodies at a concentration of 1:10,000. Protein bands were visualized using enhanced chemiluminescence (ECL, GE Healthcare) and Kodak BioMAX XAR film (Kodak). Alternatively, lysates were probed with the primary antibody and a fluorescent dye–labeled secondary antibody and images were taken using the Odyssey Infrared Imaging system from LI-COR.

Exome sequencing

BWA (Burrows-Wheeler Aligner, bio-bwa.sourceforge.net) was used to align short reads to a reference sequence (GRCh37). Duplicate sequence reads (PCR-derived duplicates) were removed from further analysis at this point. Base quality recalibration, realignment around indels, and variant calling were performed using the Genome Analysis Tool Kit (GATK) using the Broad best practice variant detection workflow (www.broadinstitute.org/gatk/guide/best-practices). Small insertions and deletions detected in the tumor cell lines that were absent in the reference genomes were considered to be candidate somatic mutations. The set of candidate somatic mutations was refined using the

Published OnlineFirst June 30, 2016; DOI: 10.1158/1535-7163.MCT-15-0554

following list of heuristic rules: (i) variants called in regions not covered by the exome capture probes were excluded; (ii) variants marked as low quality (QUAL below 20) were excluded; (iii) variants with fewer than 10 reads covering the locus in all samples were excluded. Common SNPs (those reported to have a global minor allele frequency of greater than 5% in any of the 1000 genomes project data sets) were also removed from the main analysis. The remaining variants were annotated using the Ensembl variant effect predictor script (Ensembl v61).

Cell-cycle analysis

Cells were plated at a density of 2×10^6 cells per well of a 6-well plate and incubated for 24 hours after which dasatinib or 0.1% (v/v) DMSO was added to the media and cells cultured for a further 24 hours. After incubation, both adherent and free-floating cells were harvested and then fixed overnight with cold 70% (v/v) ethanol. Cells were then treated with RNase A for 30 minutes prior to nucleic acid staining with propidium iodide (PI, Sigma). Samples were analyzed on a BD LSR II flow cytometer using BD FACSDiva software (BD Biosciences).

Apoptosis assay

After 48-hour dasatinib exposure, cells were analyzed using the ApoTox-Glo Triplex Assay (Promega) as per the manufacturer's instructions.

***In vivo* efficacy studies**

For the biomarker study, TOV21G cells were used to generate subcutaneous xenografts in *nu/nu* athymic female mice. Once tumors were established ($\geq$500 mm diameter), treatment with dasatinib was initiated for 72 hours. Dasatinib was either dissolved in 80 mmol/L sodium citrate at pH 3 for administration via oral gavage or dissolved in DMSO for intraperitoneal injections. Three animals received oral dasatinib at a dose of 15, 30, or 45 mg/kg/day and three animals received dasatinib at a dose of 5, 10 or 15 mg/kg/day i.p., the remaining animals served as a control and were not treated. Two hours after the final drug administration, animals were culled; tumor and normal tissue (spleen and liver) were then collected. Tissue was then thinly sliced and mixed with RIPA buffer in a cryotube overnight at 4°C. Samples were then homogenized and spun in a centrifuge at 15,000 rpm for 15 minutes. The supernatant was then removed and protein quantified using Bio-Rad Protein Assay Reagent (Bio-Rad).

TOV21G cells were transfected with a luciferin expression lentivirus (LVP433 Amsbio) and maintained in blasticidin selection (25 μg/mL) for 10 days prior to injection into female athymic *nu/nu* mice. A total of 1.0×10^6 TOV21G cells in 100 μL of PBS were injected directly into the peritoneal cavity of 40 *nu/nu* athymic female mice. Treatment with dasatinib ($n = 20$) or vehicle ($n = 20$) was initiated 24 hours after tumor injection. Mice received either dasatinib 15 mg/kg in sodium citrate (80 mmol/L) via oral gavage or vehicle treatment (sodium citrate) daily. Prior to IVIS imaging, luciferin 150 mg/kg (PerkinElmer) was injected into the peritoneum. Mice were culled when they exhibited signs of distress or >20% weight loss or gain (secondary to ascites).

Results

Identification of *ARID1A*-selective drugs using a focused drug screen

We aimed to identify existing drugs that could selectively target *ARID1A*-mutant OCCC. To do this, we designed a high-throughput drug sensitivity screen (Fig. 1A), where we profiled the *in vitro* sensitivity of a range of tumor cell models of OCCC to 68 drugs many of which are currently used in the treatment of cancer or are in late-stage development. To facilitate this, we first characterized a panel of commonly used OCCC tumor cell models according to their *ARID1A* gene mutation and protein expression status. Using whole exome sequencing and immunoblot analysis, we confirmed the previously documented (23, 24) presence of truncating *ARID1A* mutations and loss of full-length ARID1A protein expression in SMOV2, OVISE, TOV21G, OVTOKO, OVMANA, KOC7C, OVAS, and HCH1 OCCC cell line models (Supplementary Figs. S1A and S1B and S2; Supplementary Table S5). We also confirmed the expression of full-length ARID1A protein and the absence of *ARID1A* gene mutations in ES2, KK, and RMG-1 models of OCCC (Supplementary Figs. S1A and S1B and S2; Supplementary Table S5). This characterization allowed us to define two cohorts of OCCC tumor cell models for further analysis: *ARID1A* mutant (deficient; SMOV2, OVISE, TOV21G, OVTOKO, OVMANA, KOC7C, OVAS and HCH1) and *ARID1A* wild -type (ES2, KK, and RMG-1).

Using these OCCC tumor cell lines, we carried out a series of parallel high-throughput drug sensitivity screens (HTS). As a screening library, we used an in-house curated collection of 68 drugs that were selected on the basis of being either already used in the treatment of cancer or being in late-stage development (Supplementary Table S2). Each tumor cell line was plated in a 384-well plate format and then 24 hours later, exposed to each drug for a subsequent five days. At the end of this five-day period, we estimated cell viability by the use of a CellTiterGlo (CTG) assay (Fig. 1A). Each of the 11 OCCC tumor cell lines was screened in triplicate, with replica drug sensitivity data from each cell line being highly reproducible as shown by Pearson correlation coefficients between screen replicas of > 0.75 (Fig. 1B and Supplementary Table S6). The dynamic range of each screen was also estimated by calculating Z prime (Z') values for data from each 384-well plate used in the screen. To calculate Z' values, we compared CTG luminescent readings from DMSO (cell inhibition negative control) exposed cells to CTG luminescence readings from wells where cells were exposed to 5 μmol/L puromycin (cell inhibition–positive control). Each 384-well plate in the screen delivered a $Z' > 0.5$ (Fig. 1C; Supplementary Table S6), confirming a suitable dynamic range for each plate used in the screen. To maximize the potential for identifying *ARID1A* synthetic lethal effects, we screened each cell line using four different drug concentrations (1 nmol/L, 10 nmol/L, 100 nmol/L, and 1 μmol/L) and used these data to generate dose/response survival data for each drug in each cell line model (Supplementary Table S7). These data were then used to calculate AUC for each drug in each tumor cell line as well as SF_{50} (surviving fraction 50—the concentration of drug required to elicit a 50% inhibition of the cell population) estimates of drug sensitivity (Supplementary Fig. S3A and S3B) of each OCCC tumor cell line.

By comparing the median AUC values in *ARID1A* wild-type and mutant cohorts, we identified drugs predicted to deliver an *ARID1A*-mutant–selective effect. The most profound effect identified in this way was elicited by dasatinib (BMS-354825; Fig. 1D and E). When defining the differential drug sensitivities in *ARID1A*-mutant versus wild-type cohorts by comparing median AUC values, dasatinib showed a distinct effect, with an AUC of 4×10^{-6} in the *ARID1A*-mutant cohort versus 1×10^{-5} in the ARID1A wild-type cohort (Fig. 1D and E), an effect also observed by the

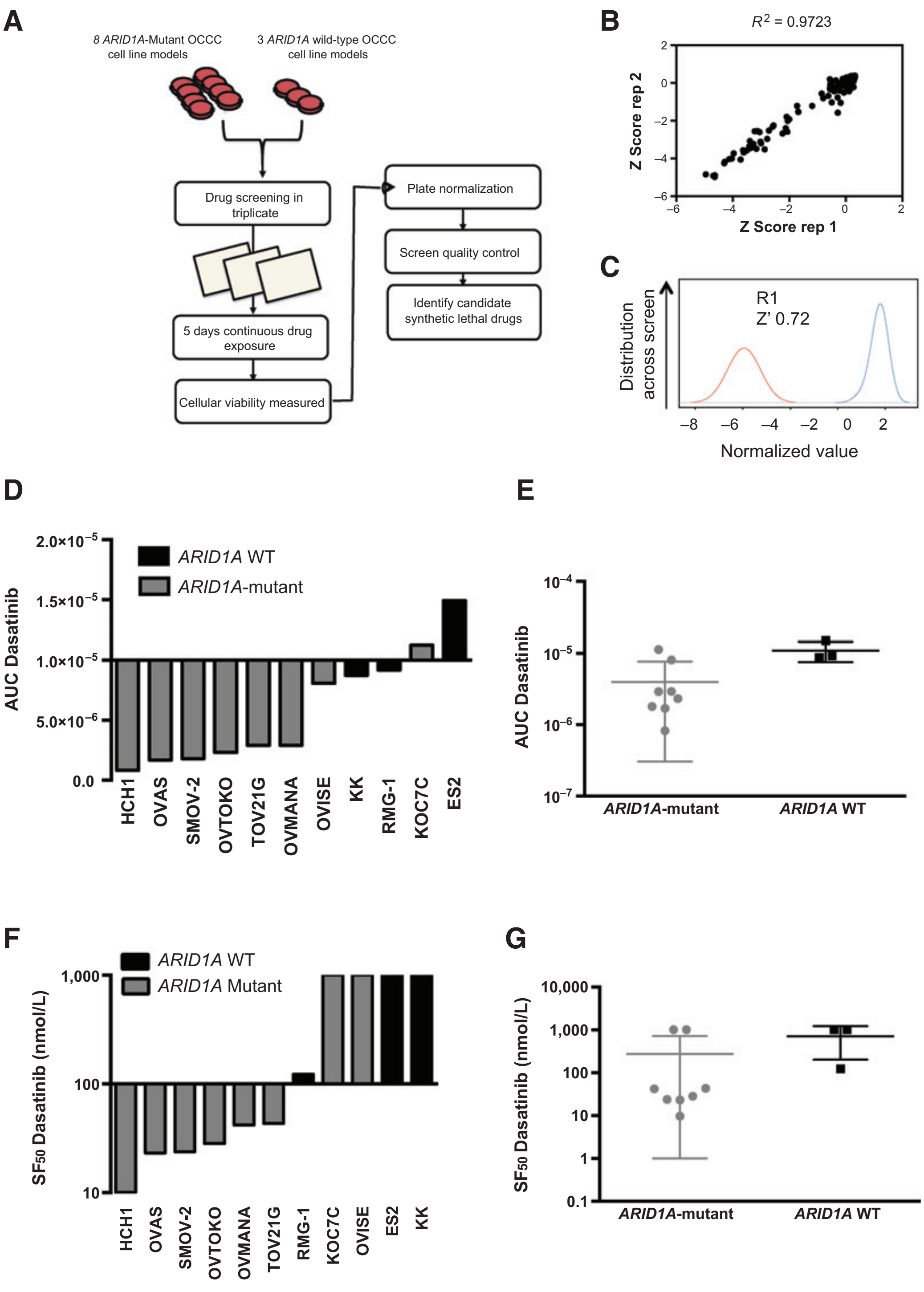

Figure 1.

Identification of *ARID1A*-selective drugs using a focused drug screen. A, focused drug high-throughput screen (HTS) schematic. Eight *ARID1A*-mutant and three *ARID1A* wild-type OCCC cell lines were plated in triplicate 384-well plates and, 24 hours later, media containing compound library were added to the 384-well plates. Cells were continuously cultured for a subsequent five days after which cell viability was estimated using a luminescence assay (CellTiter-Glo, Promega). After processing data (see Materials and Methods), the screen quality control was assessed by examining the correlation between data from replica screens (example shown in B) and Z prime statistics for each plate and each screen replica (example shown in C). B, example, scatter plot of drug sensitivity data from replica ES2 cell line screens. C, example, Z prime values for replica ES2 screens (R1 = replica 1). The distribution curve on the left represents the data from positive control (siPLK1) and the curve on the right is from negative controls (siCON). D and E, waterfall and box-whisker plots of dasatinib AUC data from the high-throughput screen. Median *ARID1A*-mutant AUC $= 4 \times 10^6$ and wild-type = AUC 1×10^5. Waterfall (F) and box-whisker (G) plots of dasatinib SF_{50} data from the high-throughput screen. Median *ARID1A* mutant $SF_{50} = 271$ nmol/L as opposed to wild-type $SF_{50} = 707$ nmol/L.

Published OnlineFirst June 30, 2016; DOI: 10.1158/1535-7163.MCT-15-0554

comparison of dasatinib SF_{50} data (Fig. 1F and G). Finally, by using an ANOVA calculation to assess the overall difference in surviving fraction across the 1 nmol/L–1 μmol/L dasatinib concentration range used in the screen, we found the *ARID1A*-mutant cohort to have a significantly lower survival that the ARID1A wild-type cohort ($P < 0.0001$, ANOVA). In addition to dasatinib, we also noted that drugs such as everolimus caused moderate *ARID1A* selective effects in the drug screen (Supplementary Table S7; Supplementary Fig. S3A). Elements of the PI3K/mTOR signaling cascade have recently been shown to be constitutively active in *ARID1A*-mutant endometrial and OCCC cancers (25–27), suggesting that *ARID1A*-mutant tumors might be addicted to PI3K signaling (28). On the basis of this earlier work and our screen data, we assessed these moderate ARID1A-selective effects in subsequent validation experiments (Supplementary Fig. S4). These confirmed that *ARID1A*-mutant tumor cell line models were modestly more sensitive to drugs such as the everolimus, but these effects were not as profound as those caused by dasatinib (Supplementary Fig. S4).

Dasatinib is a synthetic lethal drug in *ARID1A*-mutant OCCC tumor cell line models

To validate the ARID1A selectivity of dasatinib identified in the high-throughput screens, we carried out both short-term as well as long-term drug sensitivity experiments in our panel of OCCC tumor cell lines. We found that a relatively short six-day exposure to dasatinib was selective for *ARID1A*-mutant OCCC models (Fig. 2A and B and Supplementary Fig. S5A and S5B, two-way ANOVA, *ARID1A*-mutant vs. wild-type cohorts; $P < 0.05$) as was a longer-term, 15-day drug exposure (Fig. 2C and D and Supplementary Fig. S5C and S5D, two-way ANOVA, *ARID1A*-mutant vs. wild-type cohorts in Fig. 2C; $P < 0.0001$).

Although we found dasatinib to preferentially target the *ARID1A*-mutant cohort of OCCC models, the possibility existed that other genetic variants in the tumor cell line panel might explain the sensitivity to dasatinib. To independently establish whether *ARID1A* was indeed a determinant of dasatinib sensitivity, we assessed drug sensitivity in three different isogenic model systems in which we engineered either ARID1A depletion or mutation. In the first instance, we exploited the previously validated mouse ES cell model of Arid1a deficiency (Fig. 2E and Supplementary Fig. S2) generated by Gao and colleagues (9), where both alleles of *Arid1a* were rendered dysfunctional by gene targeting. We found dasatinib to be selective for the *Arid1a*-null ES cell model, compared with the wild-type clone, consistent with the hypothesis that *ARID1A* is a determinant of dasatinib sensitivity ($P < 0.0001$ two-way ANOVA; Fig. 2F). We also used gene silencing to suppress ARID1A expression in the two *ARID1A* wild-type, dasatinib-resistant, human OCCC models and *ARID1A* wild-type breast cancer and colorectal cancer cell lines models (Fig. 2G and H and Supplementary Figs. S2 and S5E–S5G). Not only did the siRNA SMARTpool designed to target ARID1A elicit dasatinib sensitivity in the *ARID1A* wild-type OCCC cell lines but this was also caused by multiple independent ARID1A siRNA species (Fig. 2G and H), suggesting that this was unlikely to be an off-target effect of the RNA interference reagents used.

In addition to these two systems of ARID1A perturbation, we also generated an isogenic human colorectal tumor cell model (HCT116) in which both copies of the *ARID1A* gene were inactivated by a p.Q456* truncating mutation. This model was generated by AAV-mediated somatic gene targeting (29). As expected, mutation of both copies of *ARID1A* (Supplementary Fig. S6A) caused loss of full-length ARID1A expression (Supplementary Figs. S2 and S6B). Using this model (*ARID1A*$^{Q456^*/Q456^*}$) and the parental ARID1A wild-type clone (*ARID1A*$^{WT/WT}$), we carried out a subsequent high-throughput drug screen using a second compound library which included the original screening library with the addition of a number of supplementary drugs (Supplementary Tables S3 and S8). Three different concentrations of dasatinib (1,000 nmol/L, 500 nmol/L, and 100 nmol/L) were ranked within the ten most profound *ARID1A*$^{Q456^*/Q456^*}$ selective effects (Supplementary Fig. S6C). This finding was confirmed in a subsequent validation assay (Supplementary Fig. S6D, two-way ANOVA, $P < 0.001$; ARID1A$^{Q456^*/Q456^*}$ cells compared with the parental *ARID1A*$^{WT/WT}$ model).

Having confirmed the validity of the ARID1A/dasatinib synthetic lethality, we assessed whether this effect could be explained by hyperactivity and/or addiction to dasatinib targets. In the first instance, we used an unbiased activity-based proteomics approach to estimate the relative activity of all dasatinib-binding kinases in a subset of our OCCC panel. This "inhibitor bead" approach is based upon the use of an ATP-competitive kinase inhibitor (in this case dasatinib) covalently linked to sepharose. As the ATP-binding avidity of protein kinases is increased by the allosteric changes that follow kinase activation, the relative amount of particular kinases bound to sepharose-dasatinib beads (measured by mass spectrometry) can be used to estimate kinase activity (Fig. 3A; refs. 19, 30, 31). Using this approach, we profiled OVISE, KK, RMG1, and TOV21G cells and found that five dasatinib targets (EPHA2, MAP4K5, ABL2, YES1, and ABL1) were significantly ($P < 0.01$) enriched in the *ARID1A*-mutant cell lines compared with the wild-type cells (Fig. 3B; Supplementary Tables S9 and S10).

Although these data suggested that *ARID1A*-mutant tumor cells exhibited enhanced activity of a number of dasatinib targets, it did not formally confirm addiction to EPHA2, MAP4K5, ABL2, YES1, or ABL1. Therefore, in parallel with this proteomic assessment, we also used a genetic approach and assessed the addiction of 10 OCCC tumor cell lines (three *ARID1A* wild-type and seven *ARID1A*-mutant models) to dasatinib targets (Fig. 3C). We selected 14 dasatinib targets that have dasatinib dissociation constants (K_d) of <1 nmol/L (32) and are inhibited at clinically relevant concentrations (ref. 33; Supplementary Table S11) and profiled each tumor cell model with this library. Using this data, we were able to calculate median NPI values for both the ARID1A-mutant OCCC cell line cohort (SMOV2, OVISE, TOV21G, OVMANA, KOC7C, OVAS, and HCH1) as well as the ARID1A wild-type cohort (KK, ES2, and RMG-1; Fig. 3C). By comparing the cell-inhibitory effects caused by each siRNA in *ARID1A* wild-type and mutant cohorts, we identified likely *ARID1A* synthetic lethal effects (Supplementary Table S11; Fig. 3D and Supplementary Fig. S7A). We noted that the most consistent *ARID1A*-selective effect (i.e., where the *ARID1A*-selective effect was observed with multiple different siRNAs) was caused by siRNA designed to target YES1 (Fig. 3D). Three of the YES1 individual siRNA species and the YES1 siRNA SMARTpool ranked within the ten most profound ARID1A-selective effects, as defined by the median difference in NPI (Fig. 3E and F and Supplementary Figs. S2 and S7B; Supplementary Table S11). We also found that the YES1 siRNA SMARTpool and individual YES1 siRNAs selectively targeted the *ARID1A*$^{Q456^*/Q456^*}$ HCT116 clone, as opposed to the *ARID1A*$^{WT/WT}$ parental clone (Supplementary Fig. S7C), suggesting that *ARID1A* mutation might indeed cause dependency upon

Published OnlineFirst June 30, 2016; DOI: 10.1158/1535-7163.MCT-15-0554

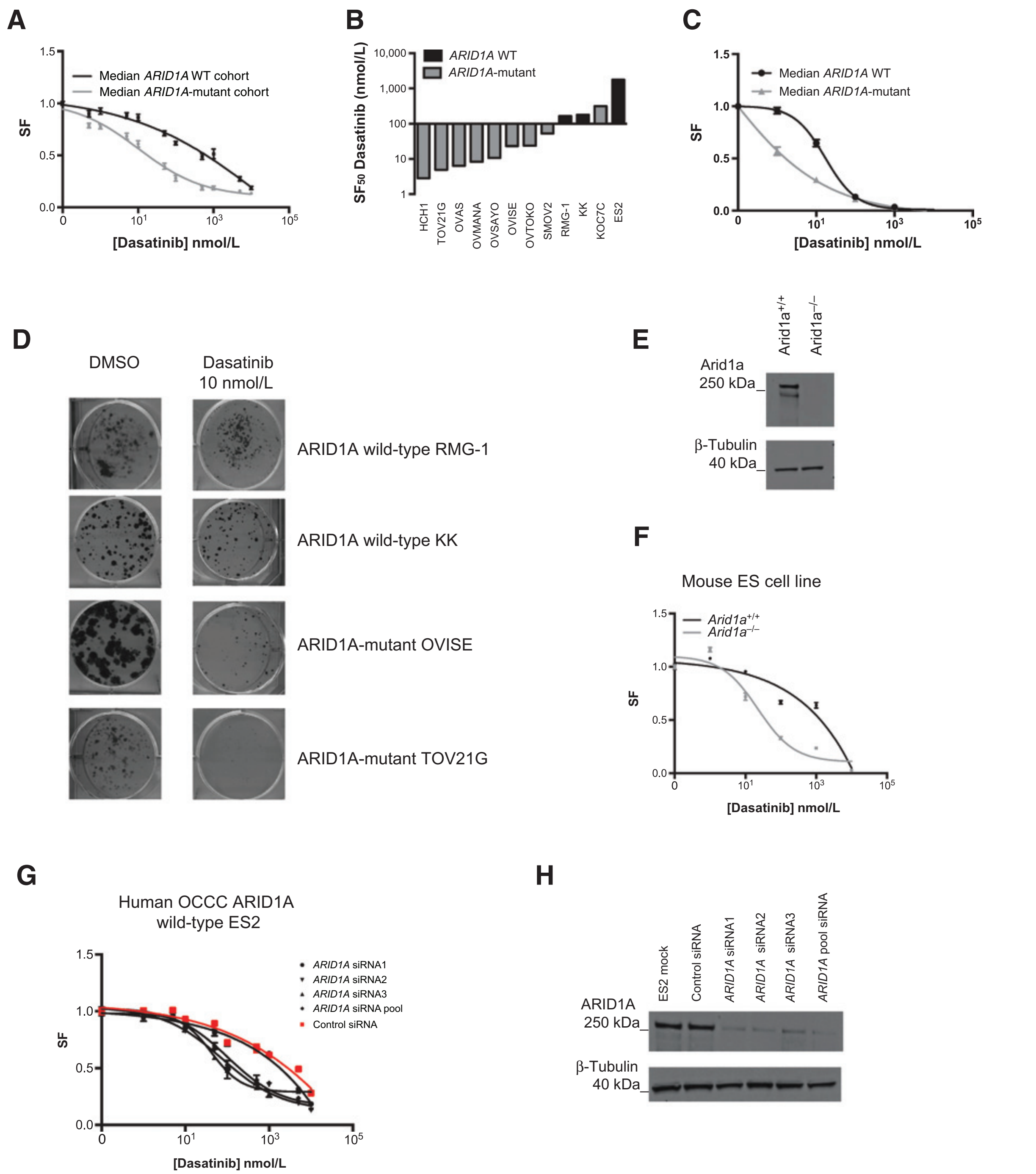

Figure 2.

Dasatinib is a synthetic lethal drug in *ARID1A* mutant OCCC tumor cell line models. A, median dasatinib SF dose–response curves in *ARID1A*-mutant and wild-type cohorts. Cells were plated in 96-well plates and exposed to dasatinib for five days after which SF were calculated. Data in A represents median of six replicates per cell line. Error bars, SEM. Dasatinib response in *ARID1A*-mutant versus wild-type cohort; two-way ANOVA, $P < 0.0001$. B, waterfall plot showing the individual dasatinib SF_{50} for each OCCC cell line (nmol/L). C, clonogenic (15-day exposure) dasatinib response in *ARID1A*-mutant *vs.* wild-type cohort; two-way ANOVA, $P < 0.0001$. D, representative clonogenic assay images from two *ARID1A* wild-type and two *ARID1A*-mutant cell lines exposed to dasatinib E, Western blot analysis of Arid1a expression from whole-cell lysates in *Arid1a* isogenic mouse ES cells. Tubulin is included as a loading control. F, dasatinib dose–response survival data from clonogenic experiments in isogenic ES cells. Cells were plated on gelatin-coated plates and exposed to dasatinib for 14 days. Error bars, SEM from six replicas per cell line. SF for the *Arid1a*-null versus *Arid1a* wild-type mouse ES cells; two-way ANOVA, $P < 0.001$. G, dasatinib dose–response survival data from the *ARID1A* wild-type cells (ES2) transfected with siRNA targeting ARID1A. Forty-eight hours after transfection, cells were plated into 96-well plates and exposed to dasatinib for five days. Error bars, SEM from six replica experiments. H, Western blot analysis of ARID1A expression from whole-cell lysates (ES2) transfected as described in G. Tubulin is included as a loading control.

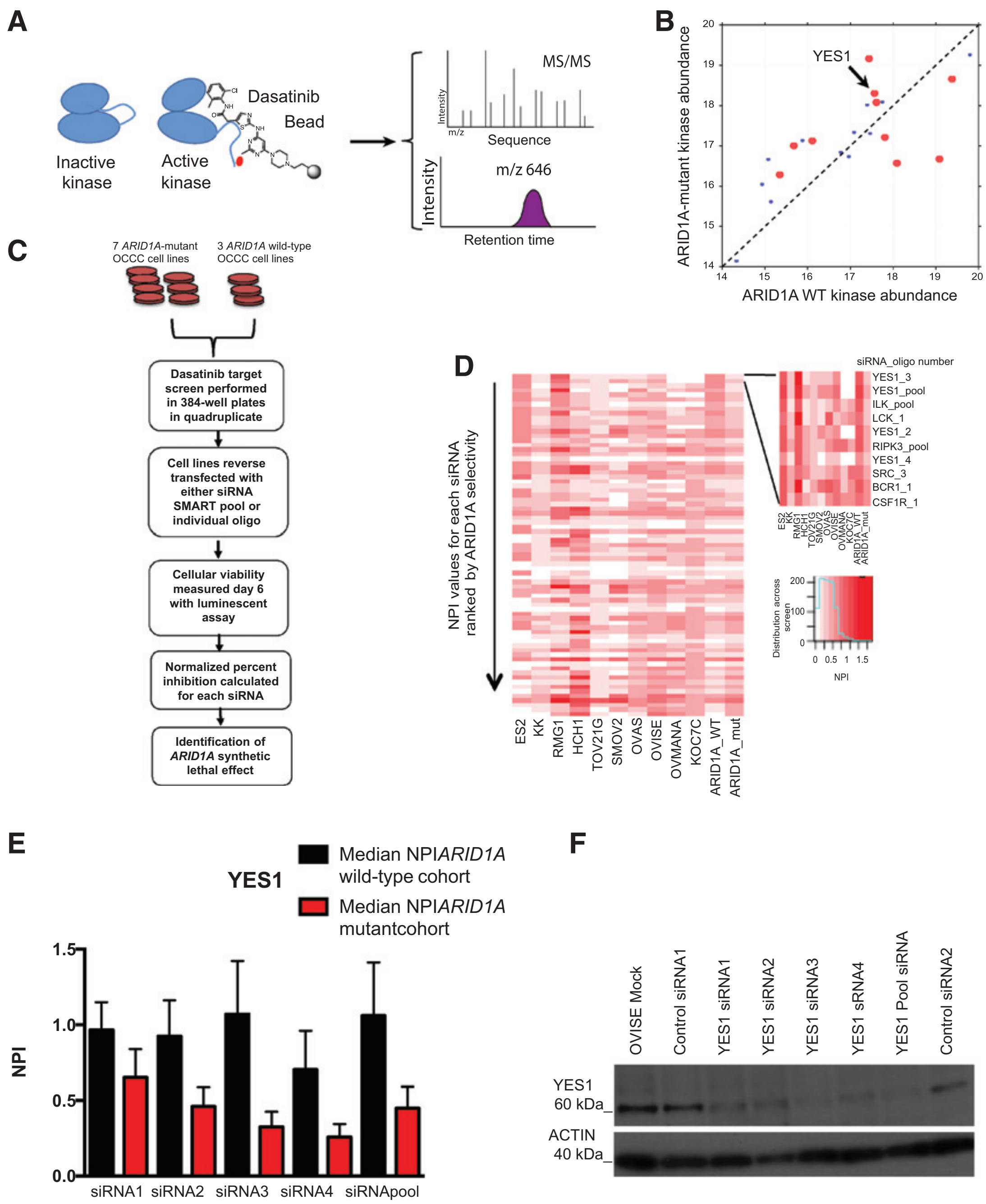

Figure 3.

ARID1A-mutant cell line models and YES1 addiction. A, schematic of inhibitor bead approach: active kinases are preferentially purified by dasatinib coupled to sepharose and analysed by LC/MS/MS. Label-free quantification with MS1 filtering is used to determine relative representation of each peptide. B, scatter plot of dasatinib-bound kinase abundance from pooled biologic replicates (two each) of *ARID1A* wild-type (KK, RMG-1) and mutant (OVISE, TOV21G) tumor cell lines. Axis represents median centered abundance; statistically significant ratios between *ARID1A*-mutant and wild-type cell lines (adjusted $P < 0.05$) are shown in red. C, dasatinib target siRNA screen overview. Ten OCCC cell lines were included in the screen. Each cell line was reverse transfected with either a SMARTpool of four siRNAs designed or individual siRNA species (four per gene) in a 384-well plate. The siRNA library targeted known targets of dasatinib. After siRNA transfection, cells were cultured for a subsequent five days at which point cell viability was estimated by the use of Cell TiterGlo Reagent. To estimate the extent to which each siRNA caused tumor cell inhibition, normalized percent inhibition (NPI) values for each siRNA were calculated and median NPI values between *ARID1A* wild-type and mutant cohorts compared. D, heatmap showing NPI data from the dasatinib target siRNA screen. Individual siRNAs are ranked according to difference in NPI between *ARID1A*-mutant and wild-type cohorts. The ten most profound *ARID1A*-selective are highlighted. E, bar chart plot of YES1 NPI values from the screen. Median NPI values from each cohort are shown; error bars, SEM. In each case, the NPI in the *ARID1A*-mutant cell line was significantly less than in the wild-type model ($P < 0.05$, Student *t* test). F, Western blot analysis demonstrating YES1 silencing caused by each individual siRNA species in the OVISE cell line. The OVISE cell line was transfected with either control siRNA, individual YES1 siRNAs, YES1 SMARTpool, or mock transfected. Forty-eight hours after transfection, whole-cell lysates were collected. Western blots were probed for YES1 and ACTIN was included as a loading control.

Published OnlineFirst June 30, 2016; DOI: 10.1158/1535-7163.MCT-15-0554

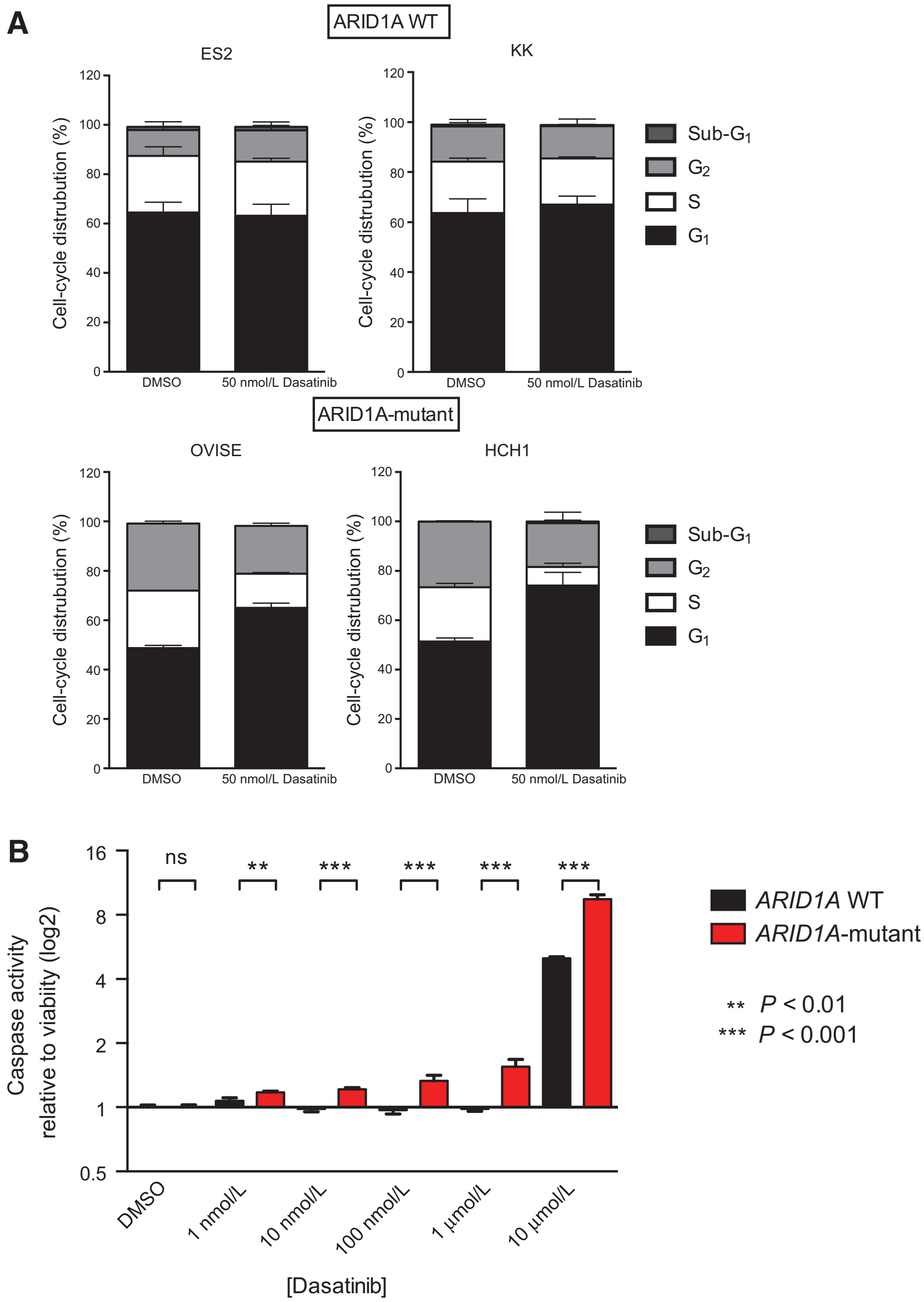

Figure 4.
Dasatinib sensitivity in *ARID1A*-mutant OCCC is characterized by G_1 arrest and an apoptotic response. A, column chart illustrating the proportion of cells in different phases of the cell cycle when exposed to dasatinib. Exposure to dasatinib led to a significant increase in the proportion of cells in the G_1 phase of the cell cycle in the *ARID1A*-mutant cell lines HCH1 and OVISE but not the *ARID1A* wild-type cell lines ES2 and KK. Cells were exposed to 50 nmol/L dasatinib for 24 hours and fixed in 70% ethanol prior to propidium iodide staining and FACS analysis. Error bars, $\pm$ SD from $n = 3$ independent experiments. S-phase fraction in *ARID1A*-mutant tumor cells is significantly reduced by dasatinib exposure (Student *t* test: $P < 0.05$, for both OVISE and HCH1). B, bar chart illustrating caspase-3/7 activity in response to dasatinib. Cells were treated as in A and caspase-3/7 activity assessed using the ApoTox Glo triplex assay (Promega). *P* values for *ARID1A*-mutant cells (OVISE and TOV21G) cells versus *ARID1A* wild-type (ES2 and KK) (***, $P < 0.001$; **, $P < 0.01$; ns, not significant; Student *t* test).

YES1, an observation that could explain the sensitivity of *ARID1A*-mutant tumor cells to dasatinib. We confirmed that YES1 activation was reduced at relevant dasatinib concentrations (Supplementary Figs. S2, S7D, and S7E). However, the addiction to YES1 in *ARDI1A*-mutant cell lines could not be explained by baseline differences in expression levels between the *ARID1A* wild-type and mutant cohorts (Supplementary Fig. S2 and S2E, S2F).

Dasatinib sensitivity in *ARID1A*-mutant OCCC is p21 and RB dependent and is characterized by an apoptotic response

One of the known phenotypic effects of dasatinib exposure in tumor cell lines is the induction of G_1 cell-cycle arrest followed by cell apoptosis (34–39). To understand whether a similar effect might explain the ARID1A/dasatinib synthetic lethality, we assessed cell-cycle progression and the extent of apoptosis in two *ARID1A*-mutant and two wild-type OCCC models. This was carried out using propidium iodide and Annexin V staining, followed by FACS. We observed a modest but significant increase in dasatinib-induced G_1 arrest in the *ARID1A*-mutant models, HCH1 and OVISE compared with wild-type models, ES2 and KK (Fig. 4A, $P < 0.05$ in each wild-type *vs.* mutant comparison, Student *t* test). There was, however, a more profound apoptotic response to dasatinib in the *ARID1A*-mutant models suggesting that although a cell-cycle response could form part of the

Published OnlineFirst June 30, 2016; DOI: 10.1158/1535-7163.MCT-15-0554

dasatinib effect, apoptosis might also play a role in the cell growth inhibition observed [*P* values for *ARID1A*-mutant cells (OVISE and TOV21G) cells versus *ARID1A* wild-type (ES2 and KK) $P <$ 0.05, Student *t*- test; Fig. 4B and Supplementary Fig. S8).

To further investigate what the key determinants of the ARID1A/dasatinib synthetic lethality might be, we used a synthetic rescue genetic screen to identify genes which when inactivated drove dasatinib resistance in ARID1A-null OCCC models. To do this, we transfected the *ARID1A*-mutant (p.542fs), dasatinib-sensitive (SF_{50} = 23 nmol/L) OVISE OCCC model with a siRNA library targeting 784 genes, predominantly protein kinase–coding genes, and assessed whether we could induce dasatinib resistance. OVISE cells were reverse transfected in 384-well plates containing the siRNA library. In total, nine replica transfections were performed. Forty-eight hours after siRNA transfection, cells were exposed to either 25 nmol/L dasatinib (three replicates), 120 nmol/L dasatinib (three replicates), or the drug vehicle DMSO (three replicates). Cells were then continuously exposed to drug for five days after which cell viability was estimated by use of a CTG assay. In cells transfected with a control nontargeting siRNA (siCON), exposure to 25 nmol/L dasatinib resulted in a SF_{50}, whereas exposure to 120 nmol/L dasatinib resulted in a SF on 16% (SF_{16}). The effect of each siRNA on dasatinib resistance was then estimated by calculating drug effect (DE) Z scores (ref. 18; see Materials and Methods) with positive DE Z scores representing resistance -causing effects. For each gene, the DE Z scores at 25 and 125 nmol/L dasatinib were calculated and rank ordered (Fig. 5A; Supplementary Table S12). By calculating the average DE Z scores from both SF_{50} and SF_{16} screens, we identified those siRNAs that elicited the most robust dasatinib resistance-causing effects.

Using this relatively unbiased approach, we found the most profound dasatinib resistance–causing effects in both SF_{50} and SF_{16} screens to be caused by siRNAs targeting the key G_1–S cell-cycle regulators *CDKN1A* (*p21*) and *RB1* (DE Z scores of 4.41 and 4.96 respectively, Fig. 5A). Dasatinib has been shown to increase the expression of p21, the protein encoded by *CDKN1A*, as well as enhancing the protein expression of another cyclin-dependent kinase inhibitor, p27 (34, 36, 38–41). Considering this, as well as the results from the synthetic rescue screen described above, we assessed whether the dasatinib/ARID1A synthetic lethality could be reversed by inactivation of *CDKN1A* or the downstream mediator, *RB1*. We found that an siRNA pool designed to target *CDKN1A* reversed the dasatinib/ARID1A synthetic lethality in the *ARID1A*-mutant OCCC cell line OVISE but had negligible effects in an *ARID1A* wild-type model ES2 (Fig. 5B and Supplementary Fig. S9A). To confirm that the dasatinib resistance observed was due to *CDKN1A* silencing and not an off-target effect, three individual siRNA species and the SMARTpool were transfected into two *ARID1A*-mutant OCCC cell lines and the *ARID1A* isogenic clones. Transfection of each individual siRNA and the SMARTpool led to dasatinib resistance in both of the cell lines examined suggesting an on-target effect (Fig. 5C) and Western blot analysis confirmed CDKN1A silencing (Fig. 5D and Supplementary Fig. S2). We also found that silencing of RB1, a key modulator of the G_1–S checkpoint also caused dasatinib resistance in multiple *ARID1A*-mutant OCC cell lines and the isogenic HCT116 *ARID1A*$^{Q456^*/Q456^*}$ clone (Supplementary Figs. S2 and S9B–S9E), supporting the hypothesis that in *ARID1A*-null tumor cells, the inhibitory effect of dasatinib is mediated via the activity of CDKN1A and RB1.

Dasatinib is selective for *ARID1A*-mutant OCC tumors *in vivo*

We generated an *in vivo* model of *ARID1A*-mutant OCCC by subcutaneously xenografting the TOV21G *ARID1A*-mutant OCCC cell line (ARID1A p.548fs/p.756fs) into immunocompromised recipient mice. This led to the growth of very aggressive, highly proliferative, subcutaneous tumors. This approach allowed us to assess the effect of dasatinib on these tumors. Published reports on the use of dasatinib in mice vary greatly in terms of the route of administration (oral gavage or intraperitoneal injections) as well as in the dasatinib dose used (42–44). Therefore, to identify a dose and route of administration that would minimize the impact of deleterious side effects while still delivering an effective dose, we first conducted a biomarker study. Subcutaneous TOV21G tumors were established in *nu/nu* athymic mice and animals were treated with dasatinib using either oral gavage or intraperitoneal (i.p.) routes of administration at a range of concentrations (oral administration of 15, 30, or 45 mg/kg per day or intraperitoneal administration of 5, 10, or 15 mg/kg per day). By estimating the extent of SRC phosphorylation as a biomarker of dasatinib activity, we were able to predict whether dasatinib elicited a mechanistic effect in both tumor and normal tissue (Supplementary Fig. S10). At each dasatinib dose tested and using either oral or intraperitoneal administration, SRC phosphorylation was completely abolished in both tumor and normal tissue (Supplementary Fig. S10) and was well tolerated in each case. We therefore selected the lowest dose of dasatinib (15 mg/kg) for subsequent studies and administered this via an oral route.

On the basis of these data, we assessed the *in vivo* antitumor efficacy of dasatinib. To do this, we first labeled *ARID1A*-mutant TOV21G cells with a luciferase-expressing construct so that we could later visualize the extent of tumor burden in live animals by the use of an In Vivo Imaging System (IVIS, PerkinElmer). These labeled cells were then xenografted into recipient mice where they generated widespread miliary (disseminated) peritoneal disease and ascites formation, reminiscent of the clinical scenario in OCCC (Fig. 6A). Treatment of these mice with dasatinib led to a significant reduction in TOV21G-related luminescence (Fig. 6A and B, $P < 0.01$ two-way ANOVA), suggesting a therapeutic response. This effect was also reflected in an increase in overall survival in the dasatinib-treated cohort of mice ($P = 0.004$; Mantel–Cox test).

Discussion

Ovarian cancer is the most lethal gynecologic malignancy. The OCCC subtype presents a particular clinical management challenge as it is invariably characterized by resistance to standard chemotherapy as well as a poor prognosis (1). In the work presented here, we have attempted to understand drug sensitivities associated with *ARID1A* mutation in OCCC by using a functional genomics approach. This has led us to the identification of dasatinib as a candidate synthetic lethal drug in *ARID1A*-mutant OCCC. Dasatinib is not only selective for *ARID1A*-mutant OCCC models, but experimental induction of ARID1A deficiency drives dasatinib sensitivity in *ARID1A* wild-type OCCC models as well as in isogenic cell systems (both mouse and human) where ARID1A has been rendered dysfunctional by gene targeting. The selectivity of dasatinib in this context appears to be characterized by a cell-cycle arrest/apoptotic phenotype, which can be reversed with silencing of either *CDKN1A* or *RB1*.

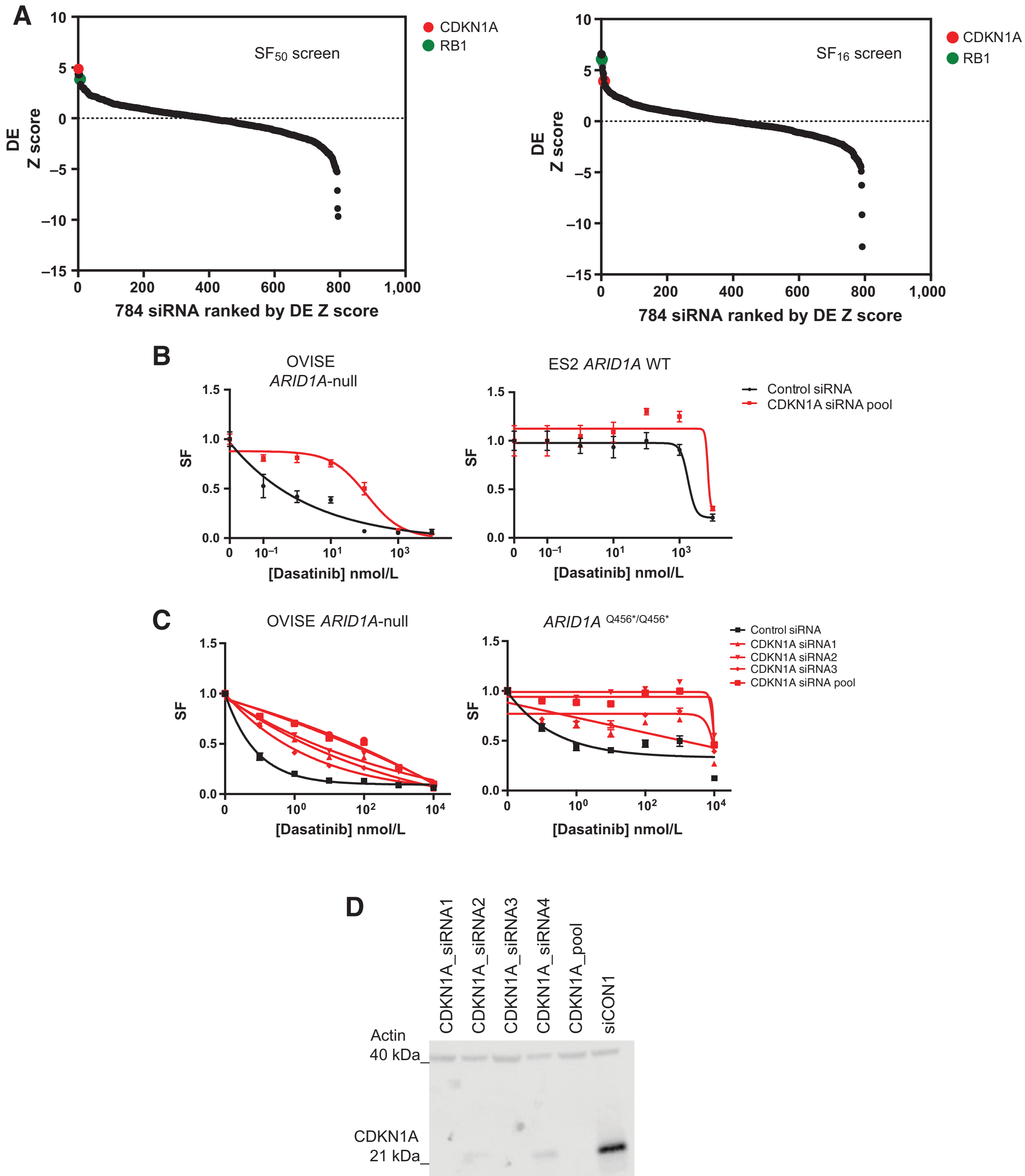

Figure 5.

Dasatinib sensitivity in *ARID1A*-mutant OCCC is dependent upon G_1–S checkpoint effectors. A, drug effect (DE) Z score distribution plots from two independent dasatinib resistance siRNA screens in OVISE tumor cells. Data from SF_{50} (left) and SF_{16} (right) dasatinib-resistant screens are shown. CDKN1A and RB1 siRNA effects are highlighted, driving dasatinib resistance in each screen. B, dasatinib dose–response curves for the *ARID1A*-mutant OCCC cell line OVISE and the *ARID1A* wild-type cell line ES2 following transfection with the CDKN1A siRNA SMARTpool. Silencing of CDKN1A expression results in dasatinib resistance. Each point represents the mean and SEM of six replicates. CDKN1A siRNA dasatinib survival curve versus control siRNA two-way ANOVA; $P < 0.0001$ for OVISE and $P = 0.02$ for ES2. C, dasatinib dose–response curves for the *ARID1A*-mutant OCCC cell line OVISE and the *ARID1A*$^{Q456*/Q456*}$ isogenic clone after transfection with four individual CDKN1A siRNA oligos and the CDKN1A SMARTpool. Each of the individual siRNAs results in dasatinib resistance suggesting that the effect observed is not due to an off-target effect. For each CDKN1A siRNA, dasatinib survival curve versus control siRNA (two-way ANOVA, $P < 0.001$). D, Western blot analysis demonstrating the on-target nature of the CDKN1A siRNA. OVISE cell line was transfected with CDKN1A siRNA and whole-cell lysates collected 48 hours later. Lysates were probed with the p21 antibody and a fluorescent dye–labeled secondary antibody used.

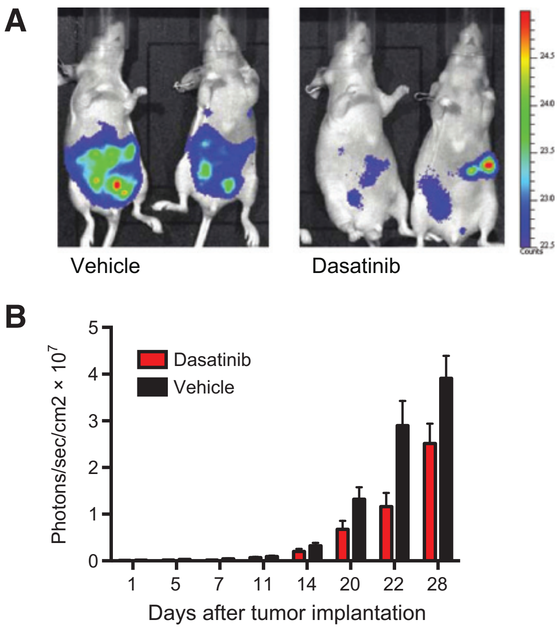

Figure 6.

In vivo assessment of *ARID1A*-mutant xenograft models. A, representative IVIS luminescent images of mice with TOV21G peritoneal xenografts after 14 days dasatinib treatment. TOV21G cells were infected with a luciferase expressing lentivector and injected into the peritoneum of BALB athymic mice ($n = 40$). Twenty-four hours later, dasatinib (15 mg/kg/day, $n = 20$) or vehicle ($n = 20$) was initiated 10 minutes prior to IVIS imaging, and mice were administered luciferin (10 μL/mg) intraperitoneally. Colored bar, photon count/cm^2/sec. B, bar chart of mean luminescence values and SEM of photons/cm^2/sec. Dasatinib-treated versus vehicle-treated (two-way ANOVA, $P < 0.01$).

ARID1A has previously been demonstrated to act as a negative regulator of the cell cycle (10, 24, 45). In part, this effect has been ascribed to an impairment of p21-mediated cell-cycle control in ARID1A-null cells (24). Taking this into account, along with the data presented here, and the known role of dasatinib in p21 induction (34, 36, 46), one possibility is that dasatinib targets *ARID1A*-mutant tumor cells because it reverses p21 dysfunction caused by ARID1A deficiency. The work presented here suggests that the dasatinib sensitivity of ARID1A-null models is somewhat dependent upon p21 and RB1, observations that are consistent with this hypothesis. It is possible that the sensitivity to dasatinib might be related to a dependency upon the dasatinib target YES1 that we have observed, although we cannot discount the possibility that other dasatinib targets might also be involved or that combinations of dasatinib targets might play a role in the phenotype we observe. We do note that an analysis of microarray-based mRNA profiles from the ARID1A wild-type and mutant tumor cell lines described in this report and publicly available transcriptomic profiles of *ARID1A*-mutant OCCC did not identify a canonical signaling process that was distinct between wild-type and mutant cohorts (R.E. Miller, C.J. Lord, A. Ashworth, unpublished observations). Although the correlation between *ARID1A* genotype and dasatinib sensitivity are striking, being present in not only in the panel of OCCC models but also in isogenic systems, we noted that one of the *ARID1A*-mutant OCCC cell lines, KOC7C, was relatively resistant to dasatinib but addicted to YES1. It is possible that while the ARID1A defect in KOC7C is sufficient to drive YES1 addiction, other genetic or epigenetic factors in this cell line modulate the ARID1A/dasatinib synthetic lethality.

Our assessment of dasatinib efficacy suggests that there are promising signs that dasatinib can inhibit *ARID1A*-mutant tumors *in vivo*, although it is clear that further work is required to optimize how dasatinib might be used to elicit a profound, long-lasting antitumor response in women with OCCCs. For example, using additional OCCC cell lines (both *ARID1A* wild-type and mutant) as established orthotopic tumors (as opposed to nonestablished tumors shown in Fig. 6) would extend the observations made using the TOV21G model. It also seems reasonable to suggest that combination therapy approaches involving dasatinib might be used to maximize the therapeutic window as well as minimizing the impact of signaling feedback loops that might impair the therapeutic effect of dasatinib. In this regard, one clear objective for future *in vivo* assessment will be to assess the possibility that the therapeutic window caused by dasatinib could be enhanced by combining this kinase inhibitor with other proposed ARID1A synthetic lethal drugs such as EZH2 and PARP inhibitors (14, 15). It might also be pertinent to assess the impact of tumor heterogeneity on the dasatinib therapeutic response. In this case, subsequent studies assessing the effect of dasatinib in mice bearing *ARID1A*-mutant human patient derived xenografts (PDX) might be appropriate, given that PDX material has the capacity to reflect the molecular heterogeneity of human tumors.

Dasatinib is already licensed for use for the treatment of chronic myelogenous leukemia (CML) and Philadelphia chromosome–positive acute lymphoblastic leukemia (AML; refs. 47, 48). Several clinical trials have also been conducted, or are at least underway, in patients with solid tumors. In these solid tumor clinical trials, dasatinib is being assessed either as a single-agent therapy or is being assessed when used in combination with cytotoxic or other targeted therapies (49). However, to date, there has been limited success in using dasatinib in the treatment of ovarian cancer patients. When dasatinib was assessed as a single-agent therapy in patients with relapsed epithelial ovarian cancer, minimal antitumor activity was observed, although we note there were only two patients with OCCC in this study, neither of which had known *ARID1A* status (50, 51). In a recent phase I clinical trial using dasatinib in combination with standard cytotoxic chemotherapy (carboplatin and paclitaxel), the drug combination regime could be delivered safely and some evidence of clinical efficacy was achieved (50, 51). Of course, neither of these trials were designed to test the hypothesis that *ARID1A*-mutant OCCC might respond to dasatinib therapy and based upon the work we describe in this manuscript, we believe that testing this hypothesis is warranted.

Disclosure of Potential Conflicts of Interest

No potential conflicts of interest were disclosed.

Authors' Contributions

Conception and design: J.D. Gordan, C.J. Lord, A. Ashworth
Development of methodology: H. Astley, C. Mahoney, C. Torrance, K.M. Shokat, C.J. Lord
Acquisition of data (provided animals, acquired and managed patients, provided facilities, etc.): R.E. Miller, I. Bajrami, C.T. Williamson, S. McDade, A. Kigozi, H. Pemberton, R. Natrajan, J. Joel, H. Astley, C. Mahoney, J.D. Moore, J.D. Gordan, R.S. Levin, C.J. Lord

Analysis and interpretation of data (e.g., statistical analysis, biostatistics, computational analysis): R.E. Miller, I. Bajrami, C.T. Williamson, J. Campbell, J.D. Gordan, J.T. Webber, R.S. Levin, K.M. Shokat, S. Bandyopadhyay, C.J. Lord, A. Ashworth

Writing, review, and/or revision of the manuscript: R.E. Miller, J.D. Moore, J.D. Gordan, K.M. Shokat, C.J. Lord, A. Ashworth

Administrative, technical, or material support (i.e., reporting or organizing data, constructing databases): R. Brough, I. Bajrami, A. Kigozi, R. Rafiq

Study supervision: C.J. Lord, A. Ashworth

Acknowledgments

The authors thank Prof. Stan Kaye (ICR and Royal Marsden Hospital, London, United Kingdom) for useful discussions and Dr. Zhong Wang (Harvard Medical School, Boston, MA) for providing *Arid1a*-null and wild-type mouse ES cells.

Grant Support

This work was supported by grants to A. Ashworth and C.J. Lord from Cancer Research UK (C347/A8363), Breast Cancer Now, and the European Union as part of the EUROCAN FP7 Programme (HEALTH-FP7-2010-260791).

The costs of publication of this article were defrayed in part by the payment of page charges. This article must therefore be hereby marked *advertisement* in accordance with 18 U.S.C. Section 1734 solely to indicate this fact.

Received July 6, 2015; revised April 4, 2016; accepted April 6, 2016; published OnlineFirst June 30, 2016.

References

1. Anglesio MS, Carey MS, Kobel M, Mackay H, Huntsman DG. Clear cell carcinoma of the ovary: a report from the first Ovarian Clear Cell Symposium, June 24th, 2010. Gynecol Oncol 2011;121:407–15.
2. Chan JK, Teoh D, Hu JM, Shin JY, Osann K, Kapp DS. Do clear cell ovarian carcinomas have poorer prognosis compared to other epithelial cell types? A study of 1411 clear cell ovarian cancers. Gynecol Oncol 2008;109:370–6.
3. Pectasides D, Fountzilas G, Aravantinos G, Kalofonos C, Efstathiou H, Farmakis D, et al. Advanced stage clear-cell epithelial ovarian cancer: the Hellenic Cooperative Oncology Group experience. Gynecol Oncol 2006; 102:285–91.
4. Jones S, Wang TL, Shih Ie M, Mao TL, Nakayama K, Roden R, et al. Frequent mutations of chromatin remodeling gene ARID1A in ovarian clear cell carcinoma. Science 2010;330:228–31.
5. Wiegand KC, Shah SP, Al-Agha OM, Zhao Y, Tse K, Zeng T, et al. ARID1A mutations in endometriosis-associated ovarian carcinomas. N Engl J Med 2010;363:1532–43.
6. Gao J, Aksoy BA, Dogrusoz U, Dresdner G, Gross B, Sumer SO, et al. Integrative analysis of complex cancer genomics and clinical profiles using the cBioPortal. Sci Signal 2013;6:pl1.
7. Katagiri A, Nakayama K, Rahman MT, Rahman M, Katagiri H, Nakayama N, et al. Loss of ARID1A expression is related to shorter progression-free survival and chemoresistance in ovarian clear cell carcinoma. Mod Pathol 2012;25:282–8.
8. Wilson BG, Roberts CW. SWI/SNF nucleosome remodellers and cancer. Nat Rev Cancer 2011;11:481–92.
9. Gao X, Tate P, Hu P, Tjian R, Skarnes WC, Wang Z. ES cell pluripotency and germ-layer formation require the SWI/SNF chromatin remodeling component BAF250a. Proc Natl Acad Sci U S A 2008;105:6656–61.
10. Nagl NGJr, Patsialou A, Haines DS, Dallas PB, Beck GRJr, Moran E. The p270 (ARID1A/SMARCF1) subunit of mammalian SWI/SNF-related complexes is essential for normal cell cycle arrest. Cancer Res 2005;65:9236–44.
11. Weissman B, Knudsen KE. Hijacking the chromatin remodeling machinery: impact of SWI/SNF perturbations in cancer. Cancer Resarch 2009;69: 8223–30.
12. Inoue H, Furukawa T, Giannakopoulos S, Zhou S, King DS, Tanese N. Largest subunits of the human SWI/SNF chromatin-remodeling complex promote transcriptional activation by steroid hormone receptors. J Biol Chem 2002;277:41674–85.
13. Lemon B, Inouye C, King DS, Tjian R. Selectivity of chromatin-remodelling cofactors for ligand-activated transcription. Nature 2001;414:924–8.
14. Bitler BG, Aird KM, Garipov A, Li H, Amatangelo M, Kossenkov AV, et al. Synthetic lethality by targeting EZH2 methyltransferase activity in ARID1A-mutated cancers. Nat Med 2015;21:231–8.
15. Shen J, Peng Y, Wei L, Zhang W, Yang L, Lan L, et al. ARID1A deficiency impairs the DNA damage checkpoint and sensitizes cells to PARP inhibitors. Cancer Discov 2015;5:752–67.
16. Helming KC, Wang X, Wilson BG, Vazquez F, Haswell JR, Manchester HE, et al. ARID1B is a specific vulnerability in ARID1A-mutant cancers. Nat Med 2014;20:251–4.
17. Ashworth A, Lord CJ, Reis-Filho JS. Genetic interactions in cancer progression and treatment. Cell 2011;145:30–8.
18. Lord CJ, Martin SA, Ashworth A. RNA interference screening demystified. J Clin Pathol 2009;62:195–200.
19. Martins MM, Zhou AY, Corella A, Horiuchi D, Yau C, Rakshandehroo T, et al. Linking tumor mutations to drug responses via a quantitative chemical-genetic interaction map. Cancer Discov 2015;5:154–67.
20. Sos ML, Levin RS, Gordan JD, Oses-Prieto JA, Webber JT, Salt M, et al. Oncogene mimicry as a mechanism of primary resistance to BRAF inhibitors. Cell Rep 2014;8:1037–48.
21. Choi M, Chang CY, Clough T, Broudy D, Killeen T, MacLean B, et al. MSstats: an R package for statistical analysis of quantitative mass spectrometry-based proteomic experiments. Bioinformatics 2014;30:2524–6.
22. Brough R, Frankum JR, Sims D, Mackay A, Mendes-Pereira AM, Bajrami I, et al. Functional viability profiles of breast cancer. Cancer Discov 2011;1: 260–73.
23. Anglesio MS, Wiegand KC, Melnyk N, Chow C, Salamanca C, Prentice LM, et al. Type-specific cell line models for type-specific ovarian cancer research. PLoS One 2013;8:e72162.
24. Guan B, Wang TL, Shih Ie M. ARID1A, a factor that promotes formation of SWI/SNF-mediated chromatin remodeling, is a tumor suppressor in gynecologic cancers. Cancer Res 2011;71:6718–27.
25. Huang HN, Lin MC, Huang WC, Chiang YC, Kuo KT. Loss of ARID1A expression and its relationship with PI3K-Akt pathway alterations and ZNF217 amplification in ovarian clear cell carcinoma. Mod Pathol 2014;27:983–90.
26. Liang H, Cheung LW, Li J, Ju Z, Yu S, Stemke-Hale K, et al. Whole-exome sequencing combined with functional genomics reveals novel candidate driver cancer genes in endometrial cancer. Genome Res 2012;22:2120–9.
27. Wiegand KC, Hennessy BT, Leung S, Wang Y, Ju Z, McGahren M, et al. A functional proteogenomic analysis of endometrioid and clear cell carcinomas using reverse phase protein array and mutation analysis: protein expression is histotype-specific and loss of ARID1A/BAF250a is associated with AKT phosphorylation. BMC Cancer 2014;14:120.
28. Samartzis EP, Gutsche K, Dedes KJ, Fink D, Stucki M, Imesch P. Loss of ARID1A expression sensitizes cancer cells to PI3K- and AKT-inhibition. Oncotarget 2014;5:5295–303.
29. Khan IF, Hirata RK, Russell DW. AAV-mediated gene targeting methods for human cells. Nat Protoc 2011;6:482–501.
30. Wodicka LM, Ciceri P, Davis MI, Hunt JP, Floyd M, Salerno S, et al. Activation state-dependent binding of small molecule kinase inhibitors: structural insights from biochemistry. Chem Biol 2010;17:1241–9.
31. Bantscheff M, Eberhard D, Abraham Y, Bastuck S, Boesche M, Hobson S, et al. Quantitative chemical proteomics reveals mechanisms of action of clinical ABL kinase inhibitors. Nat Biotechnol 2007;25:1035–44.
32. Karaman MW, Herrgard S, Treiber DK, Gallant P, Atteridge CE, Campbell BT, et al. A quantitative analysis of kinase inhibitor selectivity. Nat Biotechnol 2008;26:127–32.
33. Kitagawa D, Yokota K, Gouda M, Narumi Y, Ohmoto H, Nishiwaki E, et al. Activity-based kinase profiling of approved tyrosine kinase inhibitors. Genes Cells 2013;18:110–22.
34. Guerrouahen BS, Futami M, Vaklavas C, Kanerva J, Whichard ZL, Nwawka K, et al. Dasatinib inhibits the growth of molecularly heterogeneous myeloid leukemias. Clin Cancer Res 2010;16:1149–58.
35. Inge LJ, Fowler AJ, Paquette KM, Richer AL, Tran N, Bremner RM. Dasatinib, a small molecule inhibitor of the Src kinase, reduces the growth and activates apoptosis in pre-neoplastic Barrett's esophagus cell lines: evidence

for a noninvasive treatment of high-grade dysplasia. J Thorac Cardiovasc Surg 2013;145:531–8.

36. Johnson FM, Saigal B, Talpaz M, Donato NJ. Dasatinib (BMS-354825) tyrosine kinase inhibitor suppresses invasion and induces cell cycle arrest and apoptosis of head and neck squamous cell carcinoma and non-small cell lung cancer cells. Clin Cancer Res 2005;11:6924–32.
37. Michels S, Trautmann M, Sievers E, Kindler D, Huss S, Renner M, et al. SRC signaling is crucial in the growth of synovial sarcoma cells. Cancer Res 2013;73:2518–28.
38. Song Y, Sun X, Bai WL, Ji WY. Antitumor effects of Dasatinib on laryngeal squamous cell carcinoma in vivo and in vitro. Eur Arch Otorhinolaryngol 2013;270:1397–404.
39. Le XF, Mao W, He G, Claret FX, Xia W, Ahmed AA, et al. The role of p27 (Kip1) in dasatinib-enhanced paclitaxel cytotoxicity in human ovarian cancer cells. J Natl Cancer Inst 2011;103:1403–22.
40. Le XF, Mao W, Lu Z, Carter BZ, Bast RCJr. Dasatinib induces autophagic cell death in human ovarian cancer. Cancer 2010;116:4980–90.
41. Song L, Morris M, Bagui T, Lee FY, Jove R, Haura EB. Dasatinib (BMS-354825) selectively induces apoptosis in lung cancer cells dependent on epidermal growth factor receptor signaling for survival. Cancer Res 2006;66:5542–8.
42. Chan D, Tyner JW, Chng WJ, Bi C, Okamoto R, Said J, et al. Effect of dasatinib against thyroid cancer cell lines in vitro and a xenograft model in vivo. Oncol Lett 2012;3:807–15.
43. Garcia-Gomez A, Ocio EM, Crusoe E, Santamaria C, Hernandez-Campo P, Blanco JF, et al. Dasatinib as a bone-modifying agent: anabolic and anti-resorptive effects. PLoS One 2012;7:e34914.
44. Nagathihalli NS, Merchant NB. Src-mediated regulation of E-cadherin and EMT in pancreatic cancer. Front Biosci 2012;17:2059–69.
45. Flores-Alcantar A, Gonzalez-Sandoval A, Escalante-Alcalde D, Lomeli H. Dynamics of expression of ARID1A and ARID1B subunits in mouse embryos and in cells during the cell cycle. Cell Tissue Res 2011;345: 137–48.
46. Ling C, Chen G, Chen G, Zhang Z, Cao B, Han K, et al. A deuterated analog of dasatinib disrupts cell cycle progression and displays anti-non-small cell lung cancer activity in vitro and in vivo. Int J Cancer 2012;131:2411–9.
47. Hochhaus A, Kantarjian H. The development of dasatinib as a treatment for chronic myeloid leukemia (CML): from initial studies to application in newly diagnosed patients. J Cancer Res Clin Oncol 2013;139:1971–84.
48. Liu-Dumlao T, Kantarjian H, Thomas DA, O'Brien S, Ravandi F. Philadelphia-positive acute lymphoblastic leukemia: current treatment options. Curr Oncol Rep 2012;14:387–94.
49. Puls LN, Eadens M, Messersmith W. Current status of SRC inhibitors in solid tumor malignancies. Oncologist 2011;16:566–78.
50. Schilder RJ, Brady WE, Lankes HA, Fiorica JV, Shahin MS, Zhou XC, et al. Phase II evaluation of dasatinib in the treatment of recurrent or persistent epithelial ovarian or primary peritoneal carcinoma: a Gynecologic Oncology Group study. Gynecol Oncol 2012;127:70–4.
51. Secord AA, Teoh DK, Barry WT, Yu M, Broadwater G, Havrilesky LJ, et al. A phase I trial of dasatinib, an SRC-family kinase inhibitor, in combination with paclitaxel and carboplatin in patients with advanced or recurrent ovarian cancer. Clin Cancer Res 2012;18:5489–98.

Published OnlineFirst June 30, 2016; DOI: 10.1158/1535-7163.MCT-15-0554

American Association for Cancer Research

Molecular Cancer Therapeutics

Synthetic Lethal Targeting of *ARID1A*-Mutant Ovarian Clear Cell Tumors with Dasatinib

Rowan E. Miller, Rachel Brough, Ilirjana Bajrami, et al.

Mol Cancer Ther 2016;15:1472-1484. Published OnlineFirst June 30, 2016.